

Identity-preserving Distillation Sampling by Fixed-Point Iterator

SeonHwa Kim¹ Jiwon Kim¹ Soobin Park² Donghoon Ahn¹ Jiwon Kang¹

Seungryong Kim^{3*} Kyong Hwan Jin^{1*} Eunju Cha^{2*}

¹Korea University

²Sookmyung Women's University

³KAIST

{sunkim0062, jwonkim, dhahn99, jiwon7258, kyong-jin}@korea.ac.kr,

{psb1219j, eunju.cha}@sookmyung.ac.kr, seungryong.kim@kaist.ac.kr

Abstract

Score distillation sampling (SDS) demonstrates a powerful capability for text-conditioned 2D image and 3D object generation by distilling the knowledge from learned score functions. However, SDS often suffers from blurriness caused by noisy gradients. When SDS meets the image editing, such degradations can be reduced by adjusting bias shifts using reference pairs, but the de-biasing techniques are still corrupted by erroneous gradients. To this end, we introduce Identity-preserving Distillation Sampling (IDS), which compensates for the gradient leading to undesired changes in the results. Based on the analysis that these errors come from the text-conditioned scores, a new regularization technique, called fixed-point iterative regularization (FPR), is proposed to modify the score itself, driving the preservation of the identity even including poses and structures. Thanks to a self-correction by FPR, the proposed method provides clear and unambiguous representations corresponding to the given prompts in image-to-image editing and editable neural radiance field (NeRF). The structural consistency between the source and the edited data is obviously maintained compared to other state-of-the-art methods.

1. Introduction

Diffusion models [4, 8, 9, 22, 25] have shown powerful representations on text-to-image generative tasks. With the advance of classifier guidance (CG) and classifier-free guidance (CFG) paradigms [1, 4, 8, 10], diffusion models improve the quality of generated samples [9, 25]. Such high-quality image generators can be easily extended to image editing by simply modifying forward/reverse iterations [14], applying CFG with a target prompt [2, 7] or interchanging attention layers [26].

Recently, Delta Denoising Score (DDS) [6] is proposed to edit a source image by distilling the rich generative prior

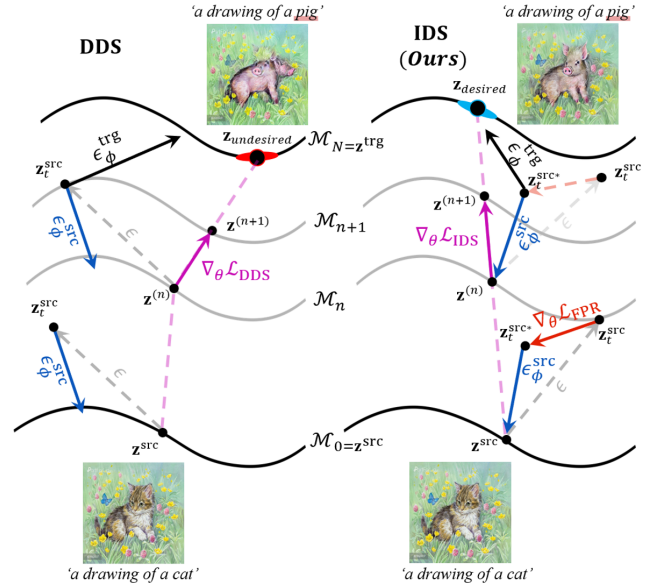


Figure 1. **Trace of guided updating** from source to target images using delta denoising score (DDS) and identity-preserving distillation sampling (IDS). DDS moves a gradient of score function toward \mathcal{M}_z manifold directed by stochastic direction ϵ . In contrast, IDS moves a gradient with a corrected direction by a fixed-point regularization.

of text-to-image diffusion models. It is based on the analysis of Score Distillation Sampling (SDS) [20], originally developed to optimize a parametric generator such as Neural Radiance Fields (NeRFs) [16] by exploiting the learned score of the diffusion models. Even though SDS offers remarkable performance in synthesizing 3D scenes, noisy gradients from stochastic perturbations lead to significantly over-saturated results that faithfully follow the given text prompts. In the context of image editing, text prompts do not often include information about the identity of the source image, such as the background, the object's pose, or the structure of the content, which should be retained during updates. Thus, DDS is designed to resolve such blurriness

*Corresponding author.

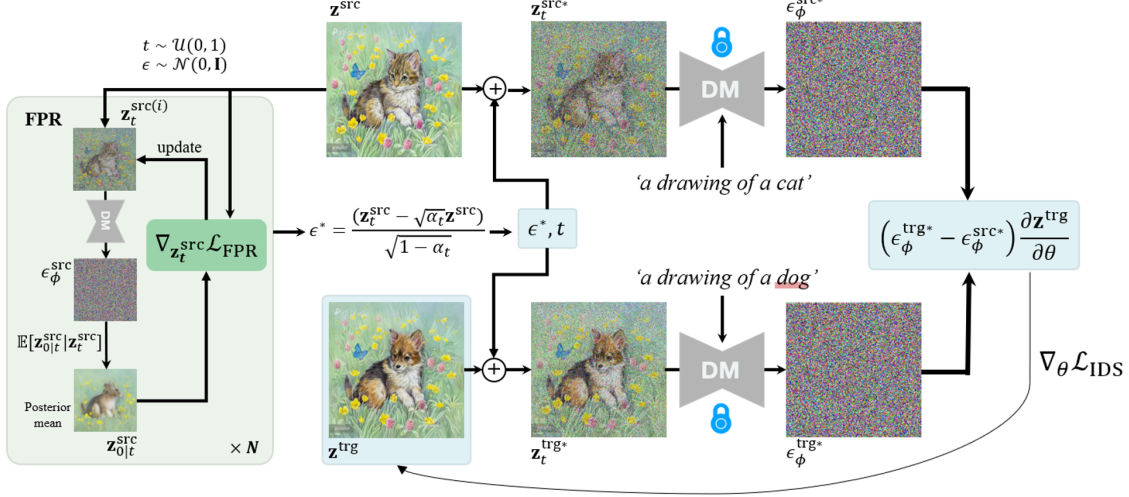


Figure 2. **Flowchart of IDS.** The backbone of our algorithm employs DDS [6] framework to distill score function into a target image. Our fixed-point regularization (FPR) obtains a guided noise, ϵ^* , from iterative updates using posterior mean computed by Tweedie’s formula. When distilling the score function to a target image, the guided noise is updated while maintaining the identity of the source.

by erasing gradients of non-text-aligned features from SDS gradients. There is no explicit procedure to preserve the source’s identity in DDS updates because the fine gradient may provide the conserved identity. However, this cannot be guaranteed if many variations in the structure are possible, such as editing the image of a cat into a pig, as shown in Fig. 1. To alleviate this problem, Contrastive Denoising Score (CDS) [17] and Posterior Distillation Sampling (PDS) [12] are introduced to maximize the mutual information of the source image and edited image. Although such algorithms rely heavily on text prompts, the algorithms have yet to analyze the inherent error caused by text-conditioned scores.

To this end, we investigate the underlying meaning of text-conditioned score. The gradient maps the stochastic latent, generated by applying the forward diffusion process to the given image, to one of the possible images described by the prompt, including the original image. Simply, the score obtained from the latent of the source image (‘source latent’) and the source prompt can be a gradient to another image represented by the identical text. Based on this interpretation, the accumulation of misaligned directions causes the loss of the source’s identity, leading to structural changes in the result with DDS, as shown in Fig. 1.

To address this issue, we propose a novel score distillation sampling to effectively preserve the identity of the original image by self-correcting the misaligned gradients, called **Identity-preserving Distillation Sampling (IDS)**. The key insight is that if the score is precisely adjusted to the source image, the conditional expectation of the source image given the source latent contains meaningful information that should be preserved during the editing. This condi-

tional expectation corresponds to the posterior mean computed by Tweedie’s formula using the learned score [3, 5]. The source latent is iteratively updated to make the posterior mean similar to the source image. This procedure, named a fixed-point iterative regularization (FPR), results in the aligned score with the source that provides reliable gradients for editing, as illustrated in Fig. 1. Following IDS update is performed using guided noise extracted from the refined source latent, rather than random Gaussian noise. This further ensures the identity preservation. Our method demonstrated superior results compared with baselines in two tasks: editing images by prompts and editing NeRF.

In summary, our main contributions are as follows:

- We obtain reliable gradients for the score distillation function by a fixed-point iterator with respect to posterior means. The iterator corrects the text-conditioned score, guiding SDS gradients toward reliable pre-trained manifolds.
- Our fixed-point regularization preserves the identities of sources such as structures and poses in edited targets. Such preservation is well demonstrated on both IoU and background PSNR between source and target.
- Our method achieves convergent target images which earn the highest score by user study and GPT compared with other score distillation methods for text-guided editing.

2. Related works

2.1. Image Editing with Diffusion Models

With the great success of image generation using diffusion models, the pre-trained diffusion models have been

recently employed for image editing tasks, demonstrating significant advancements in the quality and flexibility of generated edits [2, 7, 12, 14, 17, 26]. Stochastic Differential Editing (SDEdit) [14] is a pioneering work in which the source image was perturbed with noise, and the desired editing was achieved by gradually removing the noise through reverse stochastic differential equations. Thanks to the text-conditional Latent Diffusion Model (LDM), a.k.a. Stable Diffusion [22], text-driven editing approaches have been introduced. Specifically, the text embedding was injected through the cross-attention layer of the model for image editing and translation, while retaining the structure of the original image [7, 26]. The editing was further controlled by rescaling the attention of the specific word [7] or by manipulating the self-attention features [26]. These approaches provide greater control by balancing fidelity between the edited prompt and the source image without the need for model training, fine-tuning, additional data, or optimization. However, the current DDIM-based inversion [24] can lead to unsatisfactory reconstructions for real images, and the cross-attention bottleneck limits its effectiveness for broader edits. Crafting suitable prompts also remains challenging for complex compositions.

2.2. Score distillation sampling

Score Distillation Sampling (SDS) [20] enables text-driven 3D synthesis by leveraging probability density distillation loss to distill knowledge from 2D diffusion models, allowing high-quality 3D scene generation based on textual prompts without 3D training data. However, SDS has limitations, often producing oversaturated and overly smooth 3D models, and lacking diversity across initializations. To address these limitations of SDS, various models have been proposed based on exploiting multi-step denoising [30], a variation approach [27], negative conditioning [11], and ordinary differential equation trajectory [28]. To mitigate the limitation of noisy gradients in SDS, which hampers precise image editing, DDS [6] was introduced. By computing the delta between the derived gradient and the target pair, DDS effectively isolates and removes unwanted noise in the gradient direction. Despite these advancements, DDS still faces challenges in preserving the complete structural consistency of the source image’s identity.

3. Preliminaries

3.1. Diffusion Model and Sampling Guidance

Text-to-image diffusion models $\epsilon_\phi(\cdot)$ are based on diffusion probabilistic models (DPMs) [9, 22, 25]. The models are trained to estimate the denoising score when the original image \mathbf{z}_0 and the text condition y are given:

$$\mathcal{L}(\phi) = \mathbb{E}_{t,\epsilon} [\|\epsilon_\phi(\mathbf{z}_t, y, t) - \epsilon\|_2^2],$$

where $\epsilon \sim \mathcal{N}(0, \mathbf{I})$ and $t \sim \mathcal{U}(0, 1)$. \mathbf{z}_t refers to the stochastic latent of \mathbf{z}_0 via the forward diffusion process as follows:

$$\mathbf{z}_t = \sqrt{\alpha_t} \mathbf{z}_0 - \sqrt{1 - \alpha_t} \epsilon, \quad (1)$$

where α_t is noise schedule. With the trained $\epsilon_\phi(\cdot)$, high-quality samples can be generated using the classifier-free guidance (CFG) [8] by subtracting unconditioned denoising score from the conditioned score with guidance scale ω :

$$\epsilon_\phi^\omega(\mathbf{z}_t, y, t) = (1 + \omega) \epsilon_\phi(\mathbf{z}_t, y, t) - \omega \epsilon_\phi(\mathbf{z}_t, \emptyset, t). \quad (2)$$

3.2. Score Distillation Sampling (SDS)

With pretrained text-to-image diffusion models $\epsilon_\phi(\cdot)$, SDS [20] synthesizes 3D data \mathbf{z} for a given text prompt y by optimizing the differentiable rendering function parametrized by θ , where $\mathbf{z} = g(\theta)$:

$$\nabla_\theta \mathcal{L}_{\text{SDS}}(\mathbf{z}, y) = \mathbb{E}_{t,\epsilon} \left[\omega(t) (\epsilon_\phi^\omega(\mathbf{z}_t, y, t) - \epsilon) \frac{\partial \mathbf{z}}{\partial \theta} \right]. \quad (3)$$

The optimized parameters θ^* provide the text-conditioned 3D volume that follows the diffusion prior [20]. However, a single text prompt y can refer to many different 3D volumes, each with diverse backgrounds or structural details of the object. Therefore, an inherent limitation of SDS [20] is that the score conditioned by the prompt y does not always provide the diffusion prior to the identical object during the optimization process, leading to blurry and unclear results.

3.3. Delta Denoising Score (DDS)

DDS [6] is proposed to synthesize the image \mathbf{z}^{trg} from the given source image \mathbf{z}^{src} and its corresponding prompt y^{src} , which is aligned to the target prompt y^{trg} . Based on the insight that the gradient should be zero if y^{trg} matches y^{src} , DDS minimizes the identity change of \mathbf{z}^{src} by simple replacing ϵ in (3) with the score $\epsilon_\phi^\omega(\mathbf{z}_t^{\text{src}}, y^{\text{src}}, t)$ as follows:

$$\nabla_\theta \mathcal{L}_{\text{DDS}} = \mathbb{E}_{t,\epsilon} \left[(\epsilon_\phi^\omega(\mathbf{z}_t^{\text{trg}}, y^{\text{trg}}, t) - \epsilon_\phi^\omega(\mathbf{z}_t^{\text{src}}, y^{\text{src}}, t)) \frac{\partial \mathbf{z}^{\text{trg}}}{\partial \theta} \right]. \quad (4)$$

For simplicity, we denote $\epsilon_\phi^{\text{trg}} = \epsilon_\phi^\omega(\mathbf{z}_t^{\text{trg}}, y^{\text{trg}}, t)$ and $\epsilon_\phi^{\text{src}} = \epsilon_\phi^\omega(\mathbf{z}_t^{\text{src}}, y^{\text{src}}, t)$. Here, $\epsilon_\phi^{\text{trg}}$ and $\epsilon_\phi^{\text{src}}$ can be interpreted as the gradients representing the direction from $\mathbf{z}_t^{\text{trg}}$ to \mathbf{z}^{trg} and the direction from $\mathbf{z}_t^{\text{src}}$ to \mathbf{z}^{src} , respectively. $\theta = \mathbf{z}^{\text{trg}}$ is thus gradually optimized along the direction from \mathbf{z}^{src} to \mathbf{z}^{trg} , as shown in Fig. 1. It is worth noting that the guidance of the update can be calculated at the same point $\mathbf{z}_t^{\text{trg}}$, thanks to the shared ϵ . However, the slight error in the gradient caused by the score $\epsilon_\phi^{\text{src}}$ still leads to the incorrect direction for the optimization.

3.4. Fixed-point Iteration

In numerical analysis, a fixed-point iteration [18] is an iterative method to find fixed points of a function f , where

$f(x) = x$. Given an initial point x_0 , the iteration is defined as:

$$x_{n+1} = f(x_n), \quad n = 0, 1, 2, \dots$$

Under appropriate conditions, this sequence converges to a fixed point. Thanks to its applicability to non-linear problems with low computational costs, fixed-point iteration is widely used in optimization, including applications in the context of diffusion models [13].

4. Method

Given the source pair $\{\mathbf{z}^{\text{src}}, y^{\text{src}}\}$, the aim of our work is to provide an edited result \mathbf{z}^{trg} that is aligned with y^{trg} while maintaining the source’s identity. To this end, we introduce a novel approach called **Identity-preserving Distillation Sampling (IDS)**, which (1) corrects the error of the gradient aligned with the text prompt by the fixed-point iterator and (2) provides the result \mathbf{z}^{trg} using the guided noise.

4.1. Motivation

Analysis of the text-conditioned score. We first investigated how much identity of the given image \mathbf{z}^{src} could be contained in the text-conditioned score $\epsilon_\phi^{\text{src}}$. To do this, we conducted the experiment to compare the original image \mathbf{z}^{src} and the posterior mean $\mathbf{z}_{0|t}^{\text{src}} = \mathbb{E}[\mathbf{z}^{\text{src}} | \mathbf{z}_t^{\text{src}}]$, which is given by:

$$\mathbf{z}_{0|t}^{\text{src}} = \frac{1}{\sqrt{\alpha_t}} (\mathbf{z}_t^{\text{src}} - \sqrt{1 - \alpha_t} \epsilon_\phi^{\text{src}}), \quad (5)$$

where $\mathbf{z}_t^{\text{src}}$ denotes the source latent generated by (1). As shown in the first row of the supplementary Fig. S1, it is difficult to recognize the features of \mathbf{z}^{src} in $\mathbf{z}_{0|t}^{\text{src}}$, such as hairstyle, details of eyes, and background. This demonstrates that the score $\epsilon_\phi^{\text{src}}$ is not exactly adjusted to the given image \mathbf{z}^{src} . This deformation becomes more pronounced with increasing t . The experiment confirms that $\epsilon_\phi^{\text{src}}$ may not be a precise guidance to the source image \mathbf{z}^{src} . Therefore, the text-conditioned score $\epsilon_\phi^{\text{src}}$ needs to be modified to maintain the identity of the source image \mathbf{z}^{src} in the edited result \mathbf{z}^{trg} .

Accumulated error in DDS. The transformed image \mathbf{z}^{trg} can be converted back to the original image \mathbf{z}^{src} by reversing the set of ϵ used to synthesize \mathbf{z}^{trg} from \mathbf{z}^{src} and swapping $\{\mathbf{z}^{\text{src}}, y^{\text{src}}\}$ and $\{\mathbf{z}^{\text{trg}}, y^{\text{trg}}\}$ to calculate the DDS loss in (4). If the guidance from \mathbf{z}^{src} to \mathbf{z}^{trg} is computed exactly, the perfect reconstruction can be achieved. Nevertheless, as can be seen from the second row in Fig. 3, DDS [6] fails to restore the original image \mathbf{z}^{src} from the edited image \mathbf{z}^{trg} , which implies that the direction from \mathbf{z}^{src} to \mathbf{z}^{trg} is calculated incorrectly. Based on our analysis, this error is because the text-conditioned score $\epsilon_\phi^{\text{src}}$ do not refer to the source \mathbf{z}^{src} , which can be explicitly expressed as the difference between the injected noise ϵ and the score $\epsilon_\phi^{\text{src}}$. While the optimization is being processed, the error inevitably accumulates,

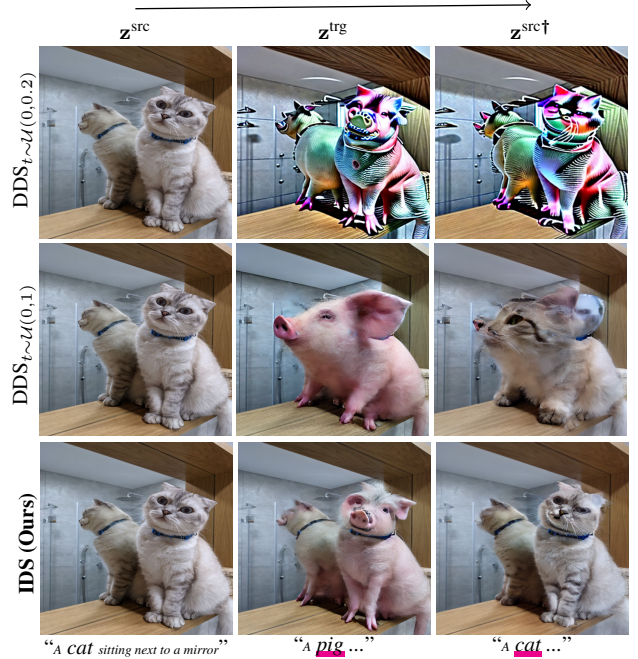


Figure 3. **Accumulated error in DDS.** \mathbf{z}^{trg} is edited image of source image \mathbf{z}^{src} by prompt $y^{\text{src}} \rightarrow y^{\text{trg}}$. $\mathbf{z}^{\text{src}\dagger}$ is the inverted image of \mathbf{z}^{trg} by prompt $y^{\text{trg}} \rightarrow y^{\text{src}}$. (First row) Inversion result of DDS with timestep $t \sim \mathcal{U}(0, 0.2)$. (Second row) Inversion result of DDS with $t \sim \mathcal{U}(0, 1)$. (Third row) Inversion result of ours.

leading to the undesirable change to the structure and the pose. To address these issues, we investigated whether the guidance from \mathbf{z}^{src} to \mathbf{z}^{trg} can be properly provided while preserving the source’s identity, when the timestep t is constrained by $t \sim \mathcal{U}(0, 0.2)$. This is because the posterior mean $\mathbf{z}_{0|t}^{\text{src}}$ and the source image \mathbf{z}^{src} are similar for small timestep t , as illustrated in the first row of supplementary Fig. S1. However, as depicted in the first row of Fig. 3, DDS yields unrealistic result with this setting, whereby the structure of the given image \mathbf{z}^{src} is overemphasized. This implies that it is not sufficient to simply limit the timestep t to prevent the score from deviating too far from \mathbf{z}^{src} to correct the misalignment of the score to \mathbf{z}^{src} . Hence, we propose a fundamental approach to refine the gradient to achieve identity consistency without unwanted overemphasis on details.

4.2. Identity-preserving Distillation Sampling (IDS)

Fixed-point Regularization (FPR). Here, we introduce a **Fixed-point Regularization (FPR)** method that adjusts the text-conditioned score $\epsilon_\phi^{\text{src}}$ to the source image \mathbf{z}^{src} . Our key premise is that if the score $\epsilon_\phi^{\text{src}}$ is rightly estimated as a gradient to \mathbf{z}^{src} , the posterior mean $\mathbf{z}_{0|t}^{\text{src}}$ also contains sufficient information about \mathbf{z}^{src} . Therefore, FPR loss is designed to minimize the difference between \mathbf{z}^{src} and $\mathbf{z}_{0|t}^{\text{src}}$ as follows:

$$\mathcal{L}_{\text{FPR}} = d(\mathbf{z}^{\text{src}}, \mathbf{z}_{0|t}^{\text{src}}), \quad (6)$$

where $d(\mathbf{x}_1, \mathbf{x}_2)$ can be any metric to compare \mathbf{x}_1 and \mathbf{x}_2 . Here, we employed the Euclidean loss, and further investigations using various metrics are provided in Supplementary Materials.

The score $\epsilon_\phi^{\text{src}}$ needs to be modified to minimize the FPR loss before obtaining the updated direction. There are two ways to control the score $\epsilon_\phi^{\text{src}}$ by altering the injection noise ϵ or the source latent $\mathbf{z}_t^{\text{src}}$. As illustrated in supplementary Fig. S1, the proposed FPR revises the score $\epsilon_\phi^{\text{src}}$ to serve the source’s identity for both approaches. Note that the score incorporates the content details, with the updates being performed with respect to the source latent $\mathbf{z}_t^{\text{src}}$ compared to the noise ϵ . Thus, $\mathbf{z}_t^{\text{src}}$ is updated to minimize the FPR loss as follows:

$$\mathbf{z}_t^{\text{src}} \leftarrow \mathbf{z}_t^{\text{src}} - \lambda \nabla_{\mathbf{z}_t^{\text{src}}} \mathcal{L}_{\text{FPR}}, \quad (7)$$

where λ and n denote a regularization scale and the number of iterations, respectively.

Algorithm 1 Fixed-point Regularization (FPR)

Require: $\mathbf{z}^{\text{src}}, y^{\text{src}}, \epsilon_\phi, \omega, \lambda, N$

- 1: $\epsilon \sim \mathcal{N}(0, \mathbf{I})$
 - 2: $t \sim \mathcal{U}(0, 1)$
 - 3: $\mathbf{z}_t^{\text{src}} \leftarrow \sqrt{\alpha_t} \mathbf{z}^{\text{src}} + \sqrt{1 - \alpha_t} \epsilon$
 - 4: **for** $i = 1, \dots, N$ **do**
 - 5: $\epsilon_\phi^{\text{src}} \leftarrow (1 + \omega) \epsilon_\phi(\mathbf{z}_t^{\text{src}}, y^{\text{src}}, t) - \omega \epsilon_\phi(\mathbf{z}_t^{\text{src}}, \emptyset, t)$
 - 6: $\mathbf{z}_{0|t}^{\text{src}} \leftarrow \frac{1}{\sqrt{\alpha_t}} (\mathbf{z}_t^{\text{src}} - \sqrt{1 - \alpha_t} \epsilon_\phi^{\text{src}})$
 - 7: $\mathcal{L}_{\text{FPR}} \leftarrow d(\mathbf{z}_{0|t}^{\text{src}}, \mathbf{z}^{\text{src}})$
 - 8: $\mathbf{z}_t^{\text{src}} \leftarrow \mathbf{z}_t^{\text{src}} - \lambda \nabla_{\mathbf{z}_t^{\text{src}}} \mathcal{L}_{\text{FPR}}$
 - 9: **end for**
 - 10: $\epsilon^* \leftarrow \frac{1}{\sqrt{1 - \alpha_t}} (\mathbf{z}_t^{\text{src}} - \sqrt{\alpha_t} \mathbf{z}^{\text{src}})$
 - 11: **return** ϵ^*
-

Editing with guided noise. Thanks to the proposed FPR, the optimized source latent $\mathbf{z}_t^{\text{src}*}$ containing the source’s identity can be obtained. Then, the guided noise ϵ^* is extracted as follows:

$$\epsilon^* = \frac{1}{\sqrt{1 - \alpha_t}} (\mathbf{z}_t^{\text{src}*} - \sqrt{\alpha_t} \mathbf{z}^{\text{src}}). \quad (8)$$

ϵ^* is utilized to produce the stochastic latent $\mathbf{z}_t^{\text{trg}*}$ by applying the forward diffusion process to the target image \mathbf{z}^{trg} . With $\mathbf{z}_t^{\text{src}*}$ and $\mathbf{z}_t^{\text{trg}*}$, the updated direction is given by:

$$\nabla_{\theta} \mathcal{L}_{\text{IDS}} = \mathbb{E}_{t, \epsilon} \left[(\epsilon_\phi^\omega(\mathbf{z}_t^{\text{trg}*}, y^{\text{trg}}, t) - \epsilon_\phi^\omega(\mathbf{z}_t^{\text{src}*}, y^{\text{src}}, t)) \frac{\partial \mathbf{z}^{\text{trg}}}{\partial \theta} \right]. \quad (9)$$

It is worth noting that ϵ^* guides the appropriate gradients for editing while conserving the source’s identity. In contrast to DDS, the proposed IDS perfectly reconstructs the source from the edited result \mathbf{z}^{trg} , as shown in the third row of Fig. 3. This confirms that the correct score and the corresponding injection noise can preserve the identity without further consideration of mutual information. The flowchart of our IDS is illustrated in Fig. 2.

5. Results

We evaluate our method through editing experiments conducted on two experiments. In Sec. 5.1, we perform a comparison on image-to-image editing across several datasets. In Sec. 5.2, we extend our evaluation to editable Neural Radiance Fields (NeRF) [16].

5.1. Text-guided image editing

Baselines. To evaluate our method, we conduct comparative experiments against four state-of-the-art image editing models: Prompt-to-Prompt (P2P) [7], Plug-and-Play (PNP) [26], DDS [6], and CDS [17]. The implementations of the baselines are carried out by referencing the official source code for each method. More details are provided in Supplementary Materials.

Qualitative Results. We present the qualitative results comparing our method with the baselines in Fig. 4. Prompt-to-Prompt (P2P) [7] performs image editing after applying DDIM inversion [4, 24] to the source image, leading to disregarding the structural components of the source image and following the target prompt excessively. Plug-and-Play (PnP) [26] has limitations in object recognition, as seen in the fourth row of Fig. 4. The third row of Fig. 4 demonstrates that DDS [6] and CDS [17] exhibited limitations, particularly in preserving the structural characteristics of the source image. In contrast, our method successfully edits the image while preserving the structural integrity of the source image.

Quantitative Results. To measure the identity-preserving performance, we utilize two datasets. First, we collect 250 cat images from the LAION 5B dataset [23] based on [17] for *Cat-to-Others* task and measure Intersection over Union (IoU). Second, we gather 28 images from the InstructPix2Pix (IP2P) dataset [2], which contains the pairs of source and target images and corresponding prompts and calculate the background Peak-Signal-to-Noise-Ratio (PSNR). Details of the metrics are provided in Supplementary Materials. In addition, we use the LPIPS score [29] for each experiment to quantify the similarity between source and target images. The results are presented in Tab. 1. Our method consistently achieves the lowest LPIPS score across all datasets, indicating that it best preserves the structural semantics of the source images.

Metric	cat2pig		cat2squirrel		lp2p	
	IoU (\uparrow)	LPIPS (\downarrow)	IoU (\uparrow)	LPIPS (\downarrow)	PSNR (\uparrow)	LPIPS (\downarrow)
P2P [7]	0.58	0.42	0.52	0.46	20.88	0.47
PnP [26]	0.55	0.52	0.53	0.52	23.81	0.39
DDS [6]	0.69	0.28	0.65	0.30	26.02	0.24
CDS [17]	0.72	0.25	0.71	0.26	27.35	0.21
IDS (Ours)	0.74	0.22	0.71	0.24	29.25	0.19

Table 1. **Quantitative results** for image editing. LPIPS [29] and IoU was measured on LAION 5B [23], while LPIPS and background PSNR was measured on InstructPix2Pix [2].

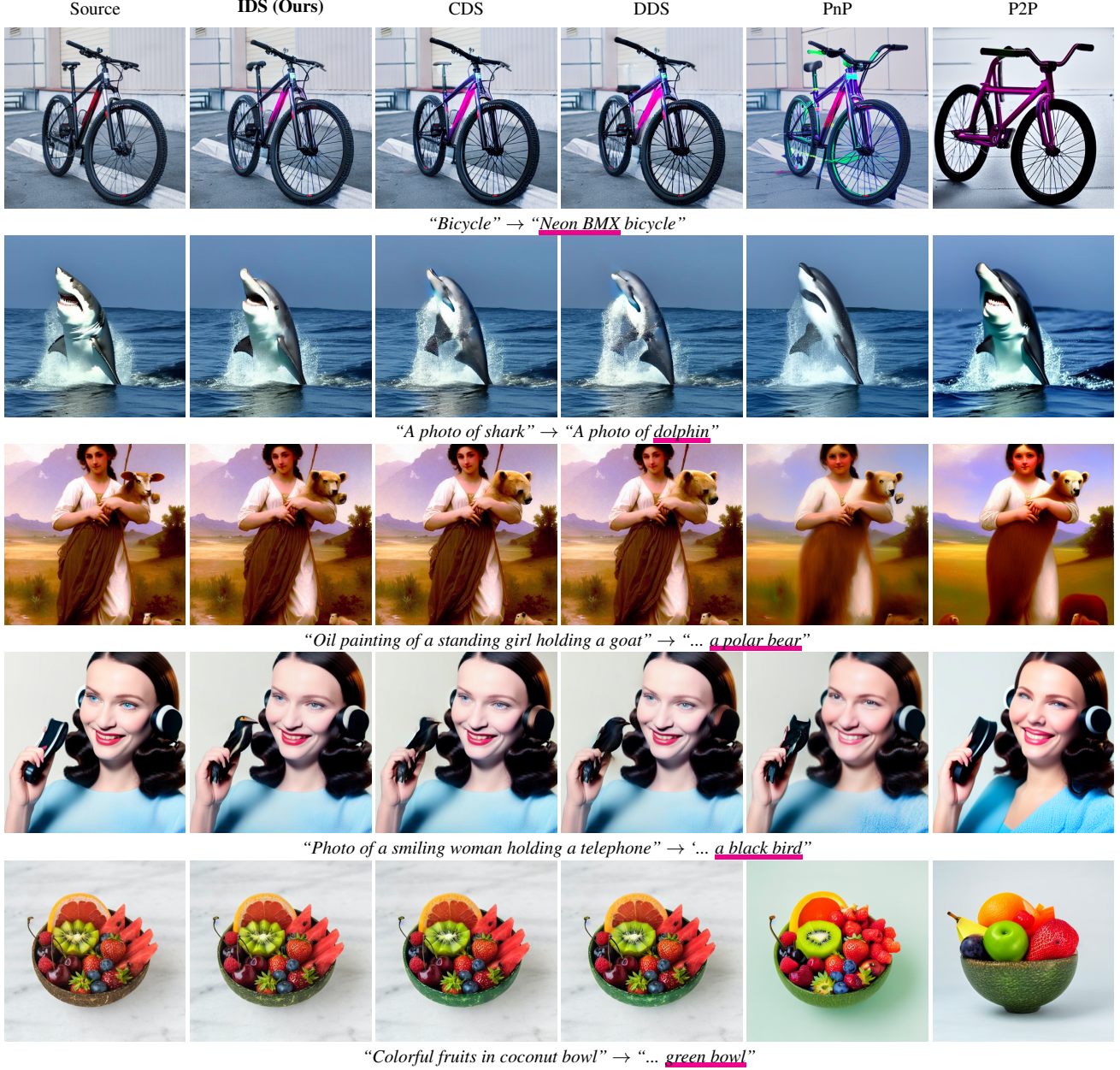


Figure 4. **Qualitative results** of InstructPix2Pix dataset [2]. Our method successfully edits the image aligning with the target text prompt while preserving the structural integrity of the source image.

For user evaluation, we present 35 comparison sets for four baselines and our method, gathering responses from 47 participants. Participants are asked to choose the most appropriate image for the following three questions: 1. *Which image best fits the text condition?* 2. *Which image best preserves the structural information of the original image?* 3. *Which image has the best quality for text-based image editing?* Additionally, we measure the GPT score using the Dreambench++ [19] method, which generates human-aligned assessments for the same questions by refining the

scoring into ten distinct levels. As shown in Tab. 2, our method receives the highest ratings for all questions.

Metric	User Preference Rate (%)			GPT score [19]		
	Text (↑)	Preserving (↑)	Quality (↑)	Text (↑)	Preserving (↑)	Quality (↑)
P2P [7]	11.13	4.80	8.09	5.66	5.37	5.77
PnP [26]	7.72	7.17	6.93	6.54	6.77	6.74
DDS [6]	20.30	10.82	16.23	7.60	7.51	7.37
CDS [17]	17.02	16.72	17.08	8.26	8.00	8.09
IDS (Ours)	43.83	60.49	51.67	8.97	9.00	8.80

Table 2. **User study and GPT scores** [19] show that our method achieved the highest scores across all questions for image editing.

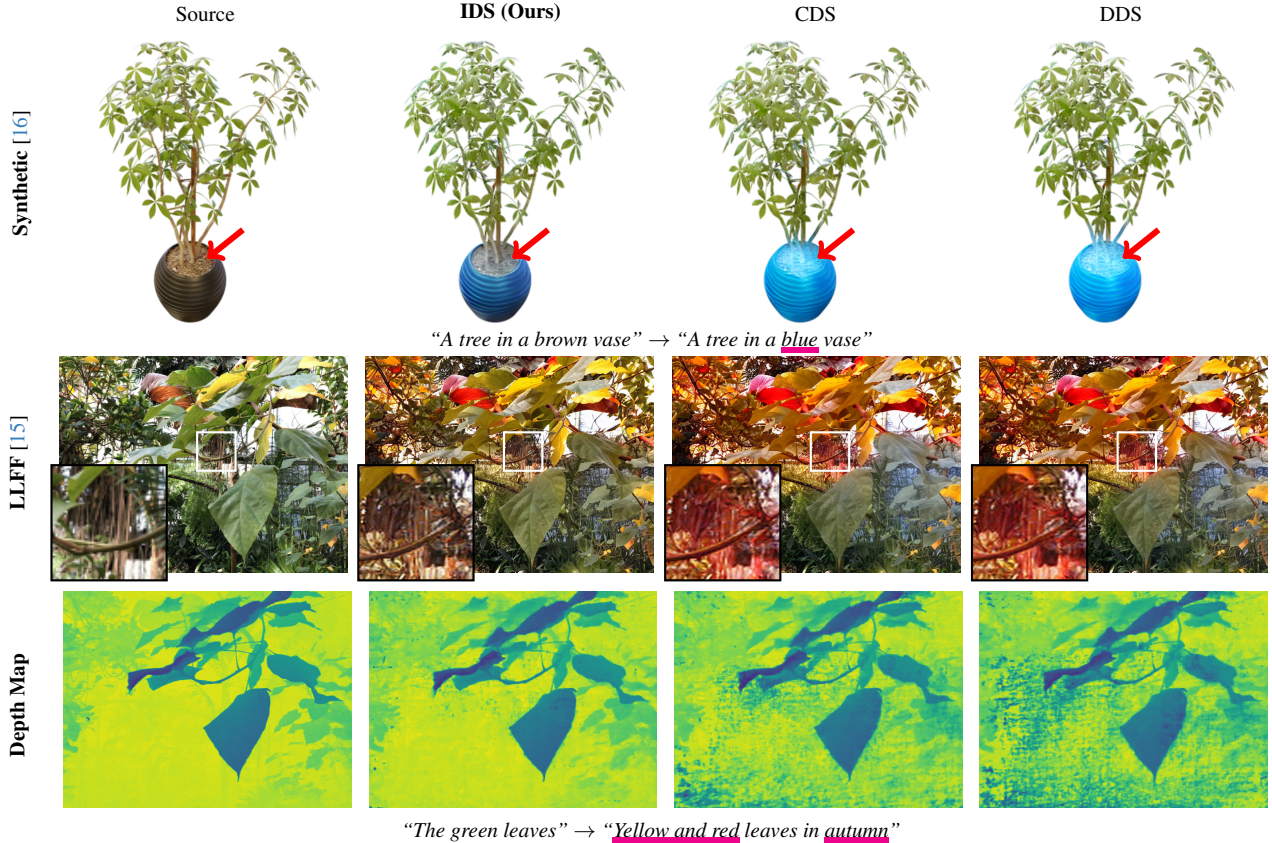


Figure 5. **Qualitative results on Synthetic 360° and LLFF datasets.** IDS outperforms the baselines by preserving the structural consistency of the source image and maintaining the integrity of regions that should remain unchanged, while precisely editing only the areas specified by the target prompt. Furthermore, comparisons of the depth map results also highlight the superior consistency of our method over other baseline models.

5.2. Editing NeRF

We conduct experiments involving 3D rendering of edited images to demonstrate the effectiveness of our method in maintaining structural consistency. This approach is particularly relevant as consistency has an even greater impact on outcomes in 3D environments.

Datasets. We evaluated our method on widely used NeRF datasets: Synthetic NeRF [16] and LLFF [15]. Since NeRF datasets have no given pairs of source and target prompts, we manually composed image descriptions, such as the source prompt “A tree in a brown vase” and its corresponding target prompt “A tree in a blue vase” as shown in Fig. 5.

Qualitative Results. Fig. 5 illustrates the qualitative results of our method compared with NeRF editing baselines. In the first row, the target prompt specifies a precise part of the image for fine-grained editing. DDS [6] and CDS [17] fail to differentiate and edit the specific area. At the same time, our method accurately identifies the region indicated

by the target prompt in the image and performs detailed editing exclusively on that part. The second row demonstrates a scenario in which the target prompt is designed to edit the mood of the image. Our approach adjusts the colors associated with “autumn” and “leaves” throughout the image while maintaining consistency in the “trunk” whereas DDS and CDS also changed the “trunk”. In terms of depth maps, our method generates clean depth maps with minimal noise after image editing, whereas DDS and CDS introduce noticeable noise into the depth maps.

Quantitative Results. Based on edited images, we performed 3D rendering and subsequently conducted quantitative evaluations provided in Tab. 3. To assess whether the edited 3D images are precisely aligned with the intended meaning of the target prompts, we measured the CLIP [21] scores at 200k iterations, where the final results on the LLFF dataset 3D renderings are saved. We additionally present a user evaluation conducted under the same setup outlined in Sec. 5.1. Consistent with the trends observed in the qualitative results, our method demonstrates supe-

rrior performance in the quantitative evaluations compared to other baselines.

Metric	CLIP [21] (\uparrow)	User Preference Rate (%)		
		Text (\uparrow)	Preserving (\uparrow)	Quality (\uparrow)
DDS [6]	0.1596	36.88	28.37	32.62
CDS [17]	0.1597	22.70	23.40	21.28
IDS (Ours)	0.1626	40.42	48.23	46.10

Table 3. **Quantitative results of NeRF editing** with respect to CLIP score and User Preference Rate. IDS demonstrates superior quantitative performance compared to the baselines.

6. Discussions

6.1. Ablation studies on FPR

Number of iterations. In the proposed FPR, the number of iterations n is one of the hyper-parameters. We conduct experiments on the number of iterations to evaluate its impact and determine the optimal iteration count. As shown in Fig. 6, the proposed FPR performs effective overall image editing with just one iteration.

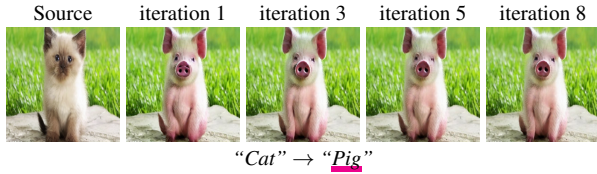


Figure 6. **Ablation study** on the number of iterations. With three or more iterations, precise image editing is achievable while preserving the structure of the source image.

Scale λ . The scaling factor λ of the FPR determines how much the source latent $\mathbf{z}_t^{\text{src}}$ is modified depending on the $d(\mathbf{z}_t^{\text{src}}, \mathbf{z}_{0|t}^{\text{src}})$. As shown in Fig. 7, increasing the scale enhances both the structural and color fidelity of the source image, highlighting the importance of the scale factor in preserving the source image’s structural attributes.

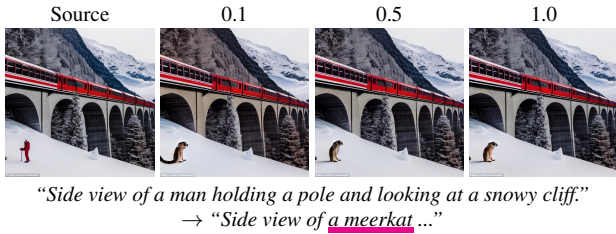


Figure 7. **Ablation study** on scale λ . For gradually increasing the scale from 0.1 to 1.0, we demonstrate that a larger scale better preserves the structure of the source image.

6.2. Optimization steps

As shown in Fig. 8, extending the number of optimization steps from 200 to 400 in DDS [6] and CDS [17] results in cumulative errors from repeated edits, leading to a degradation in structural consistency. In contrast, the proposed

IDS employs FPR to iteratively update $\mathbf{z}_t^{\text{src}}$ for the fine score $\epsilon_\phi^{\text{src}}$, effectively correcting these cumulative errors. Consequently, the capability of our approach to preserve the structural integrity of the source image during editing becomes increasingly evident.

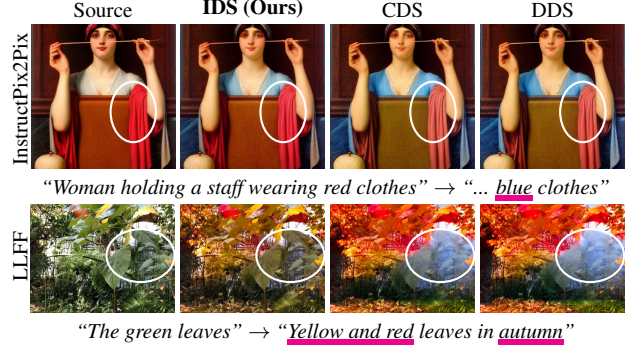


Figure 8. **Optimization steps.** Our method effectively preserves the consistency of the source image, even as the number of iteration steps increases up to 400.

7. Limitation

The proposed IDS demonstrates outstanding performance across evaluation metrics assessing consistency between source and target images. However, during FPR process, IDS relies solely on information from the source ($\{\mathbf{z}^{\text{src}}, y^{\text{src}}\}$) without incorporating target-side information. This results in comparatively lower CLIP scores [21] than other baselines as reported in Tab. 4. Our future direction will explore changing the score conditioned by the target prompt y_{trg} , leading to a better alignment with y_{trg} .

	P2P [7]	PnP [26]	DDS [6]	CDS [17]	IDS (Ours)
cat2lion	0.29	0.21	0.30	0.29	0.29
cat2dog	0.27	0.26	0.27	0.27	0.26
lp2p	0.28	0.30	0.29	0.29	0.28

Table 4. **Limitation of IDS with respect to CLIP score[21]** for image editing on LAION 5B [23] and InstructPix2Pix [2].

8. Conclusion

We proposed a new distillation sampling method using a fixed-point regularization which aligns the text-conditioned score towards identity-preserved manifolds. The proposed fixed-point regularization preserves the source’s identity by re-projecting the intermediate score status on posterior means. In this manner, corrected noises guide a gradient of distilled score toward identity-consistent manifolds. Owing to self-correction by a fixed-point iterator and guided injection noise, the proposed identity-preserving distillation sampling provides clear and unambiguous representations corresponding to the given prompts in text-guided image editing and editable neural radiance field (NeRF). Furthermore, our model can be utilized as a universal module in addition to the existing score-sampling processes.

References

- [1] Donghoon Ahn, Hyoungwon Cho, Jaewon Min, Wooseok Jang, Jungwoo Kim, SeonHwa Kim, Hyun Hee Park, Kyong Hwan Jin, and Seungryong Kim. Self-rectifying diffusion sampling with perturbed-attention guidance. *arXiv preprint arXiv:2403.17377*, 2024. 1
- [2] Tim Brooks, Aleksander Holynski, and Alexei A Efros. Instructpix2pix: Learning to follow image editing instructions. In *Proceedings of the IEEE/CVF Conference on Computer Vision and Pattern Recognition*, pages 18392–18402, 2023. 1, 3, 5, 6, 8, 2
- [3] Hyungjin Chung, Jeongsol Kim, Michael Thompson Mccann, Marc Louis Klasky, and Jong Chul Ye. Diffusion posterior sampling for general noisy inverse problems. In *The Eleventh International Conference on Learning Representations*, 2023. 2
- [4] Prafulla Dhariwal and Alexander Nichol. Diffusion models beat gans on image synthesis. *Advances in neural information processing systems*, 34:8780–8794, 2021. 1, 5
- [5] Bradley Efron. Tweedie’s formula and selection bias. *Journal of the American Statistical Association*, 106(496):1602–1614, 2011. 2
- [6] Amir Hertz, Kfir Aberman, and Daniel Cohen-Or. Delta denoising score. In *Proceedings of the IEEE/CVF International Conference on Computer Vision*, pages 2328–2337, 2023. 1, 2, 3, 4, 5, 6, 7, 8
- [7] Amir Hertz, Ron Mokady, Jay Tenenbaum, Kfir Aberman, Yael Pritch, and Daniel Cohen-or. Prompt-to-prompt image editing with cross-attention control. In *The Eleventh International Conference on Learning Representations*, 2023. 1, 3, 5, 6, 8, 4
- [8] Jonathan Ho and Tim Salimans. Classifier-free diffusion guidance. In *NeurIPS 2021 Workshop on Deep Generative Models and Downstream Applications*, 2021. 1, 3
- [9] Jonathan Ho, Ajay Jain, and Pieter Abbeel. Denoising diffusion probabilistic models. *Advances in neural information processing systems*, 33:6840–6851, 2020. 1, 3
- [10] Susung Hong, Gyuseong Lee, Wooseok Jang, and Seungryong Kim. Improving sample quality of diffusion models using self-attention guidance. In *Proceedings of the IEEE/CVF International Conference on Computer Vision*, pages 7462–7471, 2023. 1
- [11] Oren Katzir, Or Patashnik, Daniel Cohen-Or, and Dani Lischinski. Noise-free score distillation. *arXiv preprint arXiv:2310.17590*, 2023. 3
- [12] Juil Koo, Chanho Park, and Minhyuk Sung. Posterior distillation sampling. In *Proceedings of the IEEE/CVF Conference on Computer Vision and Pattern Recognition*, pages 13352–13361, 2024. 2, 3
- [13] Barak Meiri, Dvir Samuel, Nir Darshan, Gal Chechik, Shai Avidan, and Rami Ben-Ari. Fixed-point inversion for text-to-image diffusion models. *arXiv preprint arXiv:2312.12540*, 2023. 4
- [14] Chenlin Meng, Yutong He, Yang Song, Jiaming Song, Jiajun Wu, Jun-Yan Zhu, and Stefano Ermon. SDEdit: Guided image synthesis and editing with stochastic differential equations. In *International Conference on Learning Representations*, 2022. 1, 3
- [15] Ben Mildenhall, Pratul P Srinivasan, Rodrigo Ortiz-Cayon, Nima Khademi Kalantari, Ravi Ramamoorthi, Ren Ng, and Abhishek Kar. Local light field fusion: Practical view synthesis with prescriptive sampling guidelines. *ACM Transactions on Graphics (ToG)*, 38(4):1–14, 2019. 7
- [16] Ben Mildenhall, Pratul P Srinivasan, Matthew Tancik, Jonathan T Barron, Ravi Ramamoorthi, and Ren Ng. Nerf: Representing scenes as neural radiance fields for view synthesis. *Communications of the ACM*, 65(1):99–106, 2021. 1, 5, 7
- [17] Hyelin Nam, Gi Hyun Kwon, Geon Yeong Park, and Jong Chul Ye. Contrastive denoising score for text-guided latent diffusion image editing. In *Proceedings of the IEEE/CVF Conference on Computer Vision and Pattern Recognition*, pages 9192–9201, 2024. 2, 3, 5, 6, 7, 8, 4
- [18] Neal Parikh, Stephen Boyd, et al. Proximal algorithms. *Foundations and trends® in Optimization*, 1(3):127–239, 2014. 3
- [19] Yuang Peng, Yuxin Cui, Haomiao Tang, Zekun Qi, Runpei Dong, Jing Bai, Chunrui Han, Zheng Ge, Xiangyu Zhang, and Shu-Tao Xia. Dreambench++: A human-aligned benchmark for personalized image generation. *arXiv preprint arXiv:2406.16855*, 2024. 6
- [20] Ben Poole, Ajay Jain, Jonathan T Barron, and Ben Mildenhall. Dreamfusion: Text-to-3d using 2d diffusion. *arXiv preprint arXiv:2209.14988*, 2022. 1, 3
- [21] Alec Radford, Jong Wook Kim, Chris Hallacy, Aditya Ramesh, Gabriel Goh, Sandhini Agarwal, Girish Sastry, Amanda Askell, Pamela Mishkin, Jack Clark, et al. Learning transferable visual models from natural language supervision. In *International conference on machine learning*, pages 8748–8763. PMLR, 2021. 7, 8
- [22] Robin Rombach, Andreas Blattmann, Dominik Lorenz, Patrick Esser, and Björn Ommer. High-resolution image synthesis with latent diffusion models. In *Proceedings of the IEEE/CVF conference on computer vision and pattern recognition*, pages 10684–10695, 2022. 1, 3
- [23] Christoph Schuhmann, Romain Beaumont, Richard Vencu, Cade Gordon, Ross Wightman, Mehdi Cherti, Theo Coombes, Aarush Katta, Clayton Mullis, Mitchell Wortsman, et al. Laion-5b: An open large-scale dataset for training next generation image-text models. *Advances in Neural Information Processing Systems*, 35:25278–25294, 2022. 5, 8, 2
- [24] Jiaming Song, Chenlin Meng, and Stefano Ermon. Denoising diffusion implicit models. *arXiv preprint arXiv:2010.02502*, 2020. 3, 5
- [25] Yang Song, Jascha Sohl-Dickstein, Diederik P Kingma, Abhishek Kumar, Stefano Ermon, and Ben Poole. Score-based generative modeling through stochastic differential equations. *arXiv preprint arXiv:2011.13456*, 2020. 1, 3
- [26] Narek Tumanyan, Michal Geyer, Shai Bagon, and Tali Dekel. Plug-and-play diffusion features for text-driven image-to-image translation. In *Proceedings of the IEEE/CVF Conference on Computer Vision and Pattern Recognition*, pages 1921–1930, 2023. 1, 3, 5, 6, 8, 4

- [27] Zhengyi Wang, Cheng Lu, Yikai Wang, Fan Bao, Chongxuan Li, Hang Su, and Jun Zhu. Prolificdreamer: High-fidelity and diverse text-to-3d generation with variational score distillation. *Advances in Neural Information Processing Systems*, 36, 2024. [3](#)
- [28] Zike Wu, Pan Zhou, Xuanyu Yi, Xiaoding Yuan, and Hanwang Zhang. Consistent3d: Towards consistent high-fidelity text-to-3d generation with deterministic sampling prior. In *Proceedings of the IEEE/CVF Conference on Computer Vision and Pattern Recognition*, pages 9892–9902, 2024. [3](#)
- [29] Richard Zhang, Phillip Isola, Alexei A Efros, Eli Shechtman, and Oliver Wang. The unreasonable effectiveness of deep features as a perceptual metric. In *Proceedings of the IEEE conference on computer vision and pattern recognition*, pages 586–595, 2018. [5](#), [4](#)
- [30] Zhizhuo Zhou and Shubham Tulsiani. Sparsefusion: Distilling view-conditioned diffusion for 3d reconstruction. In *Proceedings of the IEEE/CVF Conference on Computer Vision and Pattern Recognition*, pages 12588–12597, 2023. [3](#)

Identity-preserving Distillation Sampling by Fixed-Point Iterator

Supplementary Material



Figure S1. **Posterior mean with/without FPR.** When the prompt y is given by “portrait of a worried-looking woman in a dress”, the posterior mean $\mathbf{z}_{0|t}$ is obtained (*first row*) without FPR, (*second row*) with FPR w.r.t \mathbf{z}_t , and (*third row*) with FPR w.r.t ϵ .

A. Posterior mean analysis

To investigate how much identity of the original image \mathbf{z} is contained in the text-conditioned score $\epsilon_\phi(\mathbf{z}, y, t)$, we conduct the experiment in which the posterior mean is obtained from various timesteps. As shown in the first row of Fig. S1, more primary information is damaged as the timestep t increases. On the other hand, when using FPR, since the score $\epsilon_\phi(\mathbf{z}, y, t)$ is modified to preserve the identity of \mathbf{z} , we can see that it has more information than before, even at large timestep, as described in the second and third row of Fig. S1. Note that the score $\epsilon_\phi(\mathbf{z}, y, t)$ can be controlled by updating the injection noise ϵ or the noisy latent \mathbf{z}_t . Of the two options, it has been updated for \mathbf{z}_t because it contains more content details.

B. Metrics for FPR



Figure S2. **Ablation study for loss function.** Edited results of (*first*) the source image from prompt “a drawing of a cat” to “a drawing of a dog” using (*second*) Euclidean, (*third*) L1, and (*fourth*) SSIM loss function for FPR.

As defined in Eq. (6), $d(\mathbf{x}_1, \mathbf{x}_2)$ can be any metric to calculate the difference between two inputs. For comparison, we consider three different strategies: (1) Euclidean loss, (2) L1 loss, and (3) SSIM loss. As demonstrated in Fig. S2, all metrics can be applied to our method for image editing according to text prompts. Among these, the use of Euclidean loss is particularly notable, as it effectively preserved the original information while producing visually superior results.

C. Implementation details

For experiments, we implement our method based on the official code of CDS¹ by using Stable Diffusion v1.4. All baselines are implemented based on the official code and setting for each method. For the proposed FPR, we set the scale λ to 1.0 and iteration N to 3. The range of timesteps, optimization, learning rate, and number of optimization steps correspond to the default settings employed in DDS and CDS. All experiments are conducted on a single NVIDIA RTX 3090.

D. Evaluation metrics

Our purpose is to preserve the source information by optimizing the score $\epsilon_\phi^{\text{src}}$. Thus, in addition to the LPIPS, we newly utilize IoU and background PSNR as our metrics to measure the structural similarity between the source and edited image.

IoU. The aim of *Cat-to-Others* task is to translate the cat into another animal. Thus, the segmentation mask of the cat and translated animal can be obtained using the language Segment-Anything model (lang-SAM)², which is an open-source project to segment some objects from the text prompt. IoU of the source and target mask represents how much the area of the cat changes after image editing. The lower the IoU, the more similar the region of the cat and the region of the translated animal, meaning the overall shape is preserved. To this end, first, the mask about the prompt is obtained from an image using lang-SAM. For example, ‘cat’ is segmented from the source image to get the mask M_{src} , while ‘dog’ is segmented from the edited image to obtain the mask M_{trg} , as shown in Fig. S3 (a). After getting masks, we calculate IoU from the masks that are given by:

$$\text{IoU} = \frac{(M_{\text{src}} \cap M_{\text{trg}})}{(M_{\text{src}} \cup M_{\text{trg}})}$$

¹<https://hyelinam.github.io/CDS/>

²<https://github.com/paulguerrero/lang-sam>

Background PSNR. Since the editing prompts of IP2P dataset [2] is complex than *Cat-to-Others* dataset [17, 23], it is hard to get mask by lang-SAM. Therefore, we use background PSNR to evaluate how much the original information is preserved. The residual of the source and target images is calculated, and the standard deviation σ of each pixel of the residual image is computed with window size 30. Then, the mask M_{PSNR} is acquired by thresholding the σ . Since the range of σ varies according to the edited results for each method, we use the mean or median values of σ to set an appropriate threshold (see Fig. S3 (b)). For the background PSNR of Tab. 1, we use mean threshold. Finally, we calculate PSNR values from masked source and target images:

$$\text{PSNR}_{\text{back}} = \text{PSNR}(M_{\text{PSNR}} \odot \mathbf{z}_{\text{src}}, M_{\text{PSNR}} \odot \mathbf{z}_{\text{trg}})$$

where \odot is pixel-wise multiplication.

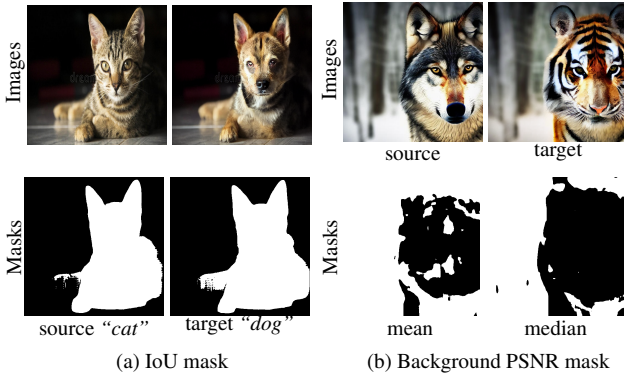


Figure S3. **Calculated masks** for IoU and background PSNR. In (a), (second row) each mask for (first row) the source and target image is obtained by using lang-SAM for IoU. In (b), (second row) a mask is calculated for (first row) the source and target image to measure background PSNR between the masked source and target image. The mask can be generated by thresholding method, mean and median

E. Extension to other methods

Since our method optimizes the source latent to estimate a more accurate score, it can be applied to other methods that are based on SDS despite that we report the results using our method to DDS.

During SDS optimization, FPR can be used to preserve the original content and reduce the blurry effect. As shown in Fig. S4, the conserved rate of the information of the source image is controllable by the number of FPR iteration.



Figure S4. **SDS with FPR.** Given (first) source image and prompt “a drawing of a cat”, (second) SDS optimization, (third, fourth) SDS optimization with FPR for 30 and 50 iterations are applied. Each result uses 200 steps for optimization.

When the proposed FPR is integrated into CDS, the texture of the source image is further maintained, as illustrated in Fig. S5. In addition, FPR promoted reducing the overboosting of color often found in the translated images of CDS. This confirms that the proposed FPR can be a universal regularization to preserve the identity of the source image for text-guided image editing.



Figure S5. **CDS with FPR.** Given (first) source image, source prompt “a drawing of a cat”, and target prompt “a drawing of a pig”, (second) CDS translation, (third) CDS optimization with FPR for $N = 3$ and $\lambda = 1.0$.

Furthermore, FPR can be helpful for optimizing not only pixel space but also the parametric editor such as PDS [12]. As demonstrated in Fig. S6, the edited results with our method show that FPR assists in maintaining the original contents. By comparing the first and second rows of Fig. S6, the use of FPR results in the preservation of source components more effectively compared to PDS. Similarly, in the third and fourth rows, the results obtained using FPR retain key original features, such as the shape and color of the face as well as the color of the clothing. Furthermore, the gradient weights, FPR assigns minimal weight to the structure of the source image, such as the background, while primarily focusing the weights on the editing points.

F. Additional results

We also provide qualitative results for *Cat-to-Others* task, as demonstrated in Fig. S7. With DDS and CDS, the direction of the gaze changes when translated from the cat to the squirrel, while it remains the same with IDS. Note that the proposed IDS can also retain the hue of the source image without overemphasizing the colors, as demonstrated in *Cat-to-Tiger* task. This confirms that the proposed IDS

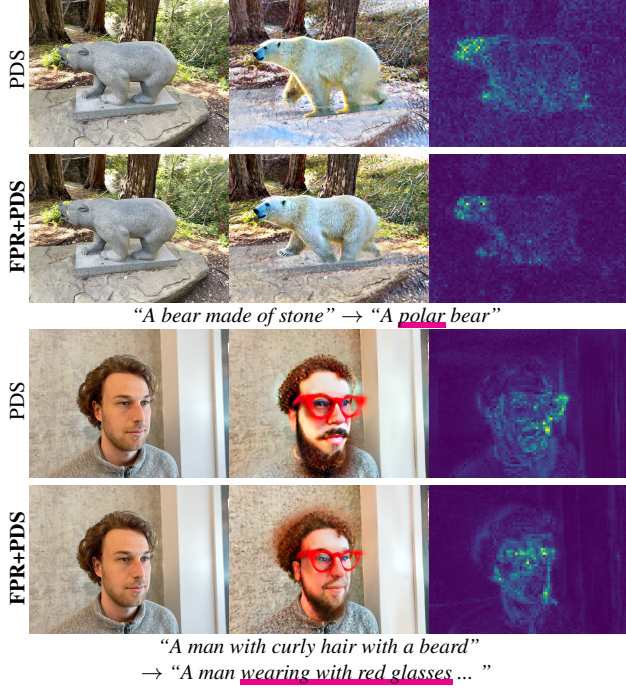


Figure S6. **Qualitative results** of the comparison between PDS and PDS with FPR. From left to right, each column represents the source image, the edited image, and the gradient weight. The gradient weight indicates which regions the model primarily references during the editing process. The results demonstrate that FPR operates effectively in End-to-End NeRF while preserving the structure and identity of the source image.

consistently offers suitable editing of cat images into the diverse animals, while conserving the identity of the source against other algorithms.

The trends in the quantitative results are also consistent with the qualitative result, as represented in Tab. S1. Our method provides the best performance for LPIPS and IoU in most *Cat-to-Others* tasks. This shows again that the self-correction of the score using the proposed algorithm is crucial for maintaining the identity.

G. Social impact

By optimizing for a given image, our method properly mitigates the undesired biases introduced by the generative priors of large text-to-image diffusion models. However, the issue of bias toward target information persists. Furthermore, the method’s potential misuse for generating fake content highlights a critical ethical challenge commonly associated with image editing techniques. To mitigate these risks, it is essential to implement robust safeguards, such as stricter content authentication mechanisms, and ethical guidelines for usage.

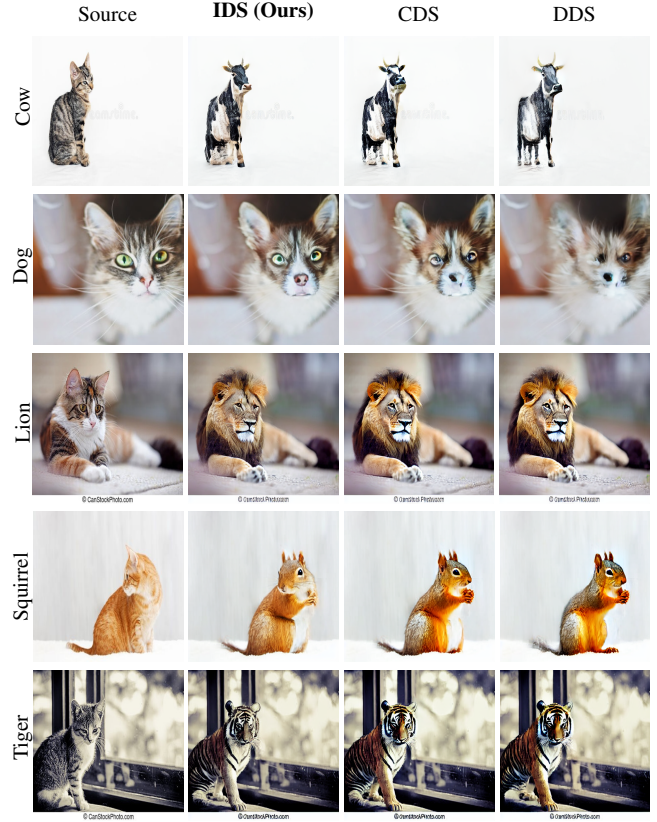


Figure S7. **Qualitative results** of *Cat-to-Others* task. The leftmost text means each target prompt, and each row shows the editing results from ‘Cat’ to the target prompt.

	cat2cow		cat2dog		cat2lion		cat2tiger		cat2penguin	
Metric	LPIPS (\downarrow)	IoU (\uparrow)	LPIPS (\downarrow)	IoU (\uparrow)	LPIPS (\downarrow)	IoU (\uparrow)	LPIPS (\downarrow)	IoU (\uparrow)	LPIPS (\downarrow)	IoU (\uparrow)
P2P [7]	0.43	0.57	0.42	0.51	0.46	0.57	0.47	0.57	0.46	0.54
PnP [26]	0.52	0.55	0.47	0.59	0.51	0.58	0.52	0.58	0.52	0.52
DDS [6]	0.29	0.65	0.22	0.72	0.29	0.69	0.30	0.71	0.28	0.66
CDS [17]	0.25	0.72	0.19	0.74	0.25	0.74	0.27	0.75	0.24	0.72
IDS (Ours)	0.21	0.74	0.17	0.75	0.21	0.71	0.21	0.76	0.21	0.72

Table S1. **Quantitative results** for *Cat-to-Others* task. LPIPS [29] and IoU are used. Lower LPIPS and higher IoU mean better identity preserving.